Degradation Study of NMC622/Graphite Second Life Li-ion Battery Packs

Lucas de O. Albuquerque[1], Eric Bru[1], Fabien Lacressonnière[1], Christophe Forgez[2], Nicolas Damay[2], Xavier Roboam[1]
[1]LAPLACE, UMR CNRS-INPT-UT, Université de Toulouse, France [2] Roberval, Université de Technologie de Compiègne, France

ABSTRACT – Understanding the aging behavior of lithium-ion battery packs is essential for optimizing system sizing and improving performance, particularly in applications involving second-life use. This study presents aging data from an accelerated cycling campaign on battery packs equipped with Battery Management Systems (BMS) featuring cell balancing functionality. A detailed analysis is conducted to quantify the impact of intercell heterogeneity, specifically capacity and resistance dispersion, on the activation of balancing circuits. The results show that increased capacity spread leads to significantly higher balancing activity and reduced available energy, emphasizing the importance of monitoring cell degradation for effective BMS design and pack utilization.

Keywords – Li-ion, Battery, Aging, Dispersion, Heterogeneity, BMS, Balancing, Second life.

1. INTRODUCTION

The subject of second-life Li-ion batteries has gained increasing attention in recent years, as they reach the end of their service life in electric vehicles and as more academic and industrial initiatives emerge [1]. Studies have shown that these batteries often retain sufficient capacity for use in less demanding applications, such as stationary microgrids coupled with decentralized energy production technologies [2]. In this context, the B2LIVE project [3] was launched to investigate the techno-economic feasibility of repurposing a specific used Li-ion battery module for microgrid applications. The project's objectives include the development of aging models for integration into microgrid simulation tools, as well as diagnostic tools for selecting suitable second-life batteries. To support this, a dedicated battery aging test bench was designed and built to evaluate and age battery packs intended for use in such applications.

This paper presents the battery aging test bench developed for the project, along with the aging test procedure applied to several batteries. Subsequently, the observed aging trends from the testing campaign are analyzed, with particular attention to the heterogeneous aging behavior seen in some modules. Finally, due to capacity dispersion among the modules, the Battery Management System (BMS) balancing circuit is frequently activated. Its behavior is examined and correlated with the aging of individual cells within a module.

2. AGING TEST BENCH AND PROTOCOL

2.1. *The battery aging test bench*

Developing an aging test bench capable of testing multiple battery packs in parallel is a complex task, as it requires monitoring numerous parameters. Moreover, continuously aging battery packs is more challenging than cell-level studies due to increased system complexity. Despite these challenges, the aging test bench developed at the LAPLACE laboratory is equipped with five DC buses, allowing the connection of batteries rated up to 400 V and 250 A. The environmental temperature of the batteries is regulated using two thermal chambers. The test bench is managed by a dSPACE supervisor, as well as the power supplies and electronic loads connected to the batteries [5]. To mitigate risks associated with lithium-ion batteries, a gas detection system is installed in each thermal chamber. The test bench includes three layers of safety, capable of shutting down individual buses, the entire system in the event of a critical issue, or injecting argon gas in case of fire.

Fig. 1 shows the battery aging test bench along with the two climate chambers, named "ETU" and "ENC", as well as an example of a battery pack. The aging campaign began in November 2023 and has been ongoing since then.

Figure 1. Battery aging test bench, battery pack and the two climate chambers.

The battery modules aged during the campaign were sourced from hybrid electric vehicles and consist of 14S NMC622/graphite pouch cells, each with a nominal capacity of 38.5 Ah. Prior to the aging campaign, a broad selection of modules was characterized to ensure the selection of similarly aged batteries for pack assembly. Fig. 2 shows the total module number as a function of median cell capacity. Since the goal was to assemble five packs with homogeneous capacities, ten modules with median capacities close to 38 Ah were selected for the study. In this configuration, two modules were connected in parallel to form 14S2P battery packs, as illustrated in Fig. 3, resulting in a total nominal capacity of 77 Ah. Each pack is equipped with a BMS to enhance safety and ensure proper cell balancing.

In this study, since the parallel-connected cells share the same voltage, each pair is treated as a single equivalent cell in the analysis. This is only valid if the currents in each of the module branches are equal, which has been monitored during the aging campaign. Periodic tests were conducted by disconnecting the parallel modules and ensuring the equilibrium of the currents.

2.2. *BMS and Cell balancing*

All cells are connected in parallel with their counterparts from the neighboring module and linked to a passive cell balancing board controlled by the BMS. This setup ensures uniform state of charge (SoC) across all 14 series-connected cell pairs and helps minimize capacity variability.

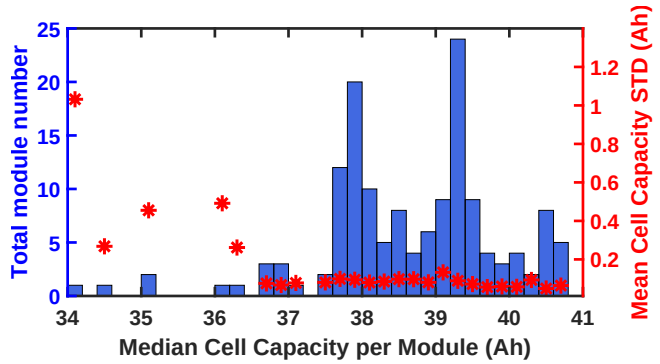

Figure 2. Battery module capacity frequency. Red start represent the mean cell capacity standard deviation (STD) of the tested modules.

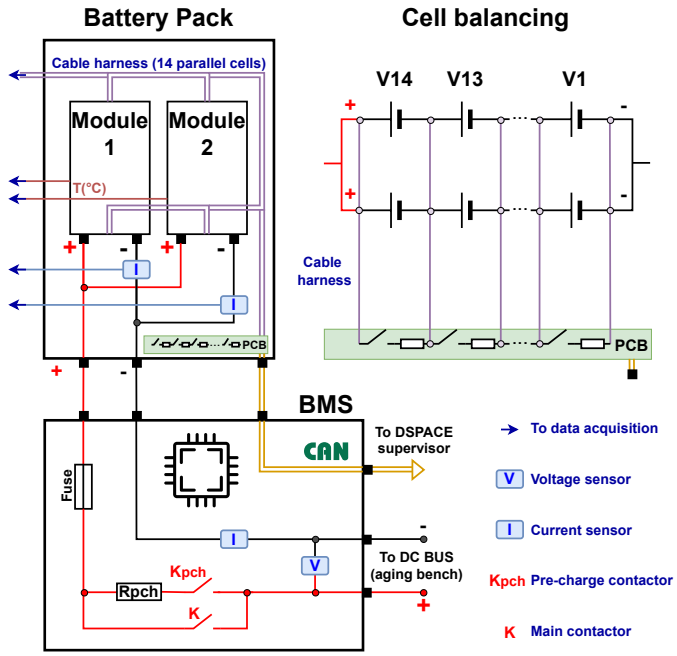

Figure 3. Battery pack, BMS and cell balancing circuit schematics.

The cell balancing board actively discharges cell pairs to equalize voltage differences between series-connected units. Each balancing pulse lasts for 10 seconds and the balancing mechanism is triggered when three conditions are met:

- Cell voltage exceeds 3.8 V.
- Current below 300 mA per cell.
- Voltage difference between any two cells exceeds 5 mV.

2.3. *The aging test procedure*

The battery packs were divided into two groups: two batteries in the ENC group, aged at 40°C, and three in the ETU group, aged at 25°C. Table 1 summarizes the aging test procedure. Initially, most of the packs began their aging profiles with an 80% Depth of Discharge (DoD), except for ENC-A, which started at 100% DoD to accelerate its degradation. Once it reached 80% State of Health (SoH), its DoD was reduced to 80%. Another variable in the aging process was the Current Rate (C-rate) applied to the batteries, which was set to 0.5C or 1C. The last battery, ETU-C, underwent aging with a self-consumption profile featuring a variable C-rate. Additionally, a 30-minute pause was imposed between each discharge and charge cycle for all batteries, except for ETU-C, which operated without any pauses. During these pauses, the BMS activates its cell balancing circuit, if necessary.

Table 1. Operating conditions of packs at different temperatures.

Temp.	Pack	SoH (%)	Profile	DoD (%)	C-rate
40°C	ENC-A	100-80	Ch. - Dch. (CC)	100	1C
		80-40	Ch. - Dch. (CC)	80	1C
	ENC-B	100-40	Ch. - Dch. (CC)	80	0.5C
25°C	ETU-A	100-40	Ch. - Dch. (CC)	80	1C
	ETU-B	100-92	Ch. - Dch. (CC)	80	0.5C
		92-40	Ch. - Dch. (CC)	50	1C
	ETU-C	100-40	Self-cons.	80	0-1.2C

As observed, the profile of ETU-B was adjusted upon reaching 92% SoH. This modification was implemented due to its aging trajectory being similar to that of other batteries in the study. The change was made during the campaign to obtain data under a different DoD.

2.4. *Characterization profile*

The batteries were periodically subjected to characterization profiles conducted at 25°C. Each profile consists of a capacity measurement using successive C/2 charge-discharge cycles, followed by a C/20 discharge-charge cycle to determine the pseudo Open Circuit Voltage (pOCV), and a pulse test at various C-rates ranging from C/5 to C for 30 seconds, performed at 50% SoC. The complete characterization profile is seen in Fig. 4.

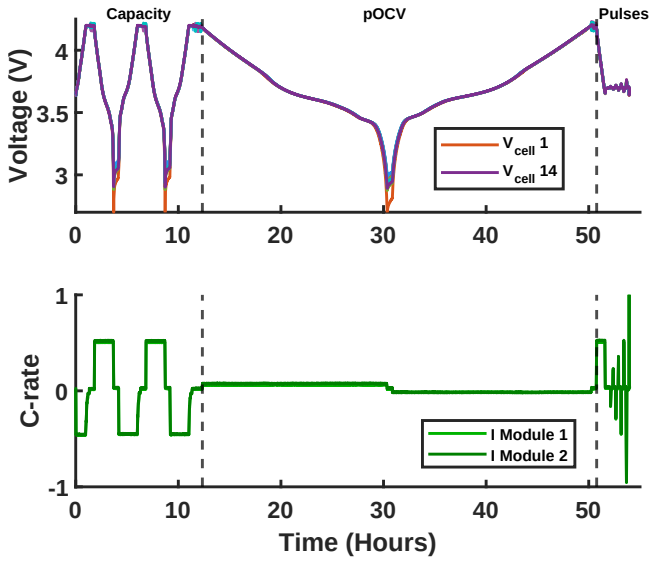

Figure 4. Characterization profile divided into three parts.

The metrics selected in this study are the SoH, degradation rate (DR), 10-second resistance, and charge-discharge efficiency. The SoH is defined as the ratio between the measured discharged capacity and the nominal capacity at C/2:

$$\text{SoH}(\%) = \frac{C_{\text{measured}}}{C_{\text{nominal}}} \cdot 100 \tag{1}$$

The degradation rate (DR) is calculated as the derivative of the SoH with respect to the ampere-hour throughput (in kAh):

$$\text{DR}\left(\frac{\%\text{SoH}}{\text{kAh}}\right) = \frac{\Delta\text{SoH}}{\Delta\text{Ah}_{\text{throughput}}} \tag{2}$$

The 10-second resistance is calculated from the voltage drop during a 1C current pulse:

$$R_{10s}(\Omega) = \frac{|V_{\text{rest}} - V_{10s}|}{I} \tag{3}$$

where V_{rest} is the voltage before the pulse, V_{10s} is the voltage after 10 seconds under current I, and the absolute value accounts for both charge and discharge pulses. The efficiency is calculated as the ratio of discharged to charged energy during the C/2 charge and discharge:

$$\eta(\%) = \frac{E_{\text{discharge}}}{E_{\text{charge}}} \cdot 100 \tag{4}$$

3. AGING CAMPAIGN RESULTS

3.1. *Battery pack level*

As a battery pack ages, the apparent measured capacity reflects the most degraded cell, which limits all other cells from reaching their minimum and maximum voltages. As shown in Fig. 5A, the aging characteristics of the five battery packs indicate that, except for ENC-A, all batteries exhibited similar aging trends. Under the selected aging conditions, neither temperature nor C-rate had a significant impact on aging, only the DoD showed a visible influence on capacity loss.

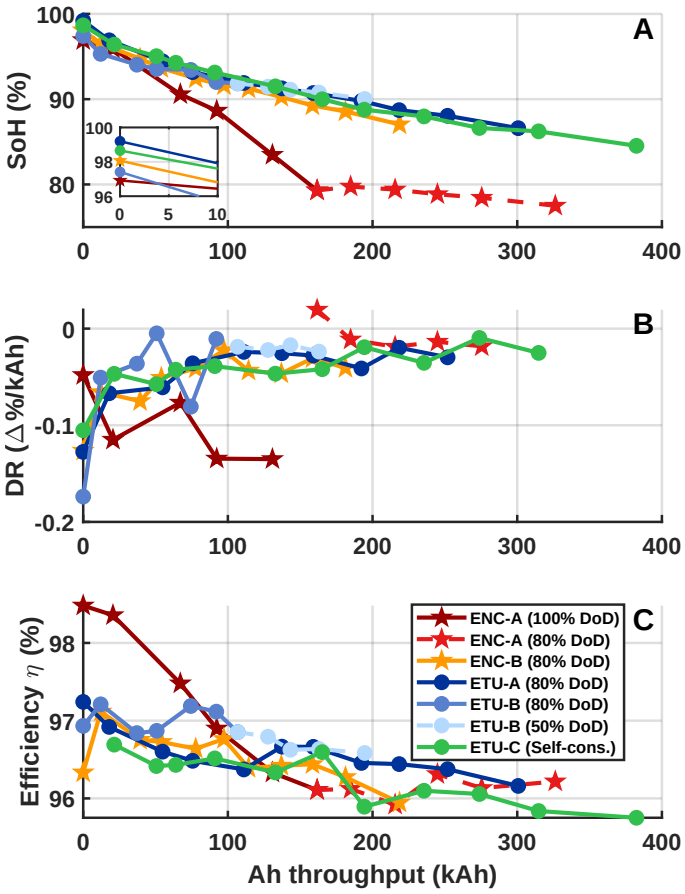

Figure 5. (A) Battery pack SoH, (B) DR and (C) efficiency η.

ENC-A exhibited its highest DR under the 100% DoD cycling profile as seen in Fig. 5B. This acceleration continued until the profile was modified, after which the pack showed a slight recovery in capacity before aligning with the degradation trends of the other batteries at the same DoD. For ETU-B, switching to a 50% DoD did not cause a notable change in its DR, and this behavior is going to be monitored as aging progresses.

The slight capacity recovery observed in ENC-A after switching from a more severe aging profile to a milder one has also been documented in the literature. For example, Gao *et al.* [6] tested multiple Nissan Leaf Gen 3 NMC cells under various aging conditions and found that aging knee effects could be reduced by limiting operating conditions, such as capping the maximum cell voltage at 4.05 V (around 80% SoC). Such slight capacity gains after profile changes have also been observed in our study.

For the other batteries, it can be observed that their DRs start off high and then quickly stabilize. This behavior can be attributed to their higher initial SoH compared to ENC-A, suggesting that their Solid Electrolyte Interphase (SEI) layers may still have been forming during the early cycles, consuming Li-ions.

Regarding energy efficiency, all batteries exhibit similar trends as seen in Fig. 5C. ENC-A initially started at a higher efficiency but rapidly converged to values comparable to the other batteries. A slight decrease in efficiency is observed with aging, however, the loss remains minimal at this stage.

3.2. *Cell level*

3.2.1. *Cell Imbalance and Its Impact on Pack Performance*

Unbalanced battery cells are known to negatively impact the total available energy within a battery pack [7]. Such imbalances may stem from various factors, including differences in cell manufacturing, temperature variations, and inconsistencies in bus bar resistance. When the SoC among cells in a pack becomes uneven, the pack's usable energy is constrained by the cells with the highest and lowest charge levels. To mitigate this, BMS have been designed to balance cell SoCs. These systems employ either passive balancing, in which excess energy is dissipated as heat via resistors, or active balancing, which transfers energy between cells and offers greater efficiency.

However, as battery packs age, the capacities and resistances of individual cells can diverge depending on the specific aging conditions. A recent study by M. Hassini [4] demonstrated that, for second-life batteries, a capacity variation of just 2% led to a 20% reduction in the pack's available energy. Moreover, variations in cell resistance were found to affect the battery's power output by up to 15%. These findings highlight the significant negative impact that cell heterogeneity can have on the overall performance of second-life battery modules.

As the battery pack becomes more heterogeneous, even if the BMS aligns the cells to the same SoC, the usable energy is still constrained by the most degraded cell. This effect is illustrated in Fig. 6, where the weakest cell limits the pack's capacity at both the upper and lower voltage thresholds. Due to its lower capacity, this cell undergoes larger SoC swings for the same Ah throughput, while the remaining cells operate over narrower DoDs, progressively increasing the disparity within the pack over time.

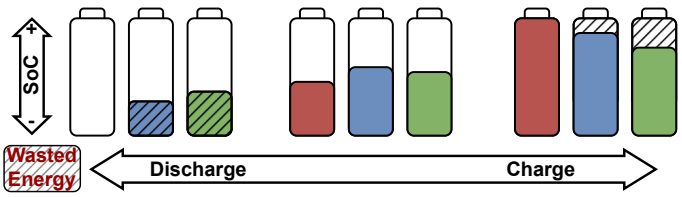

Figure 6. Heterogeneous cell capacity in a module and impact on the overall available energy. Figure inspired from [7].

To assess capacity dispersion during the aging campaign, a straightforward estimation method was applied, as shown in Fig. 7A. At the end of each discharge cycle, once the first cell dropped to 2.7 V, the remaining cells exhibit higher terminal voltages. The approach involves projecting these voltages onto the characteristic discharge curve of the limiting cell, which is the first to reach the cutoff threshold. By assuming the voltage decline of the other cells follows a similar trend, the time offset Δt is determined as the duration it would take for the limiting cell to drop from the higher voltage of each remaining cell down to 2.7 V.

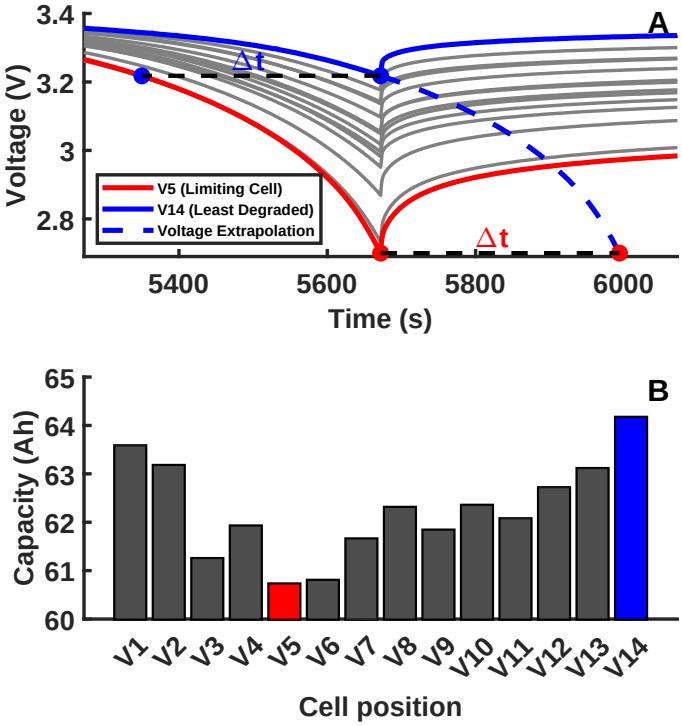

Figure 7. (A) Voltage extrapolation method and (B) individual cell capacities in the pack using the method.

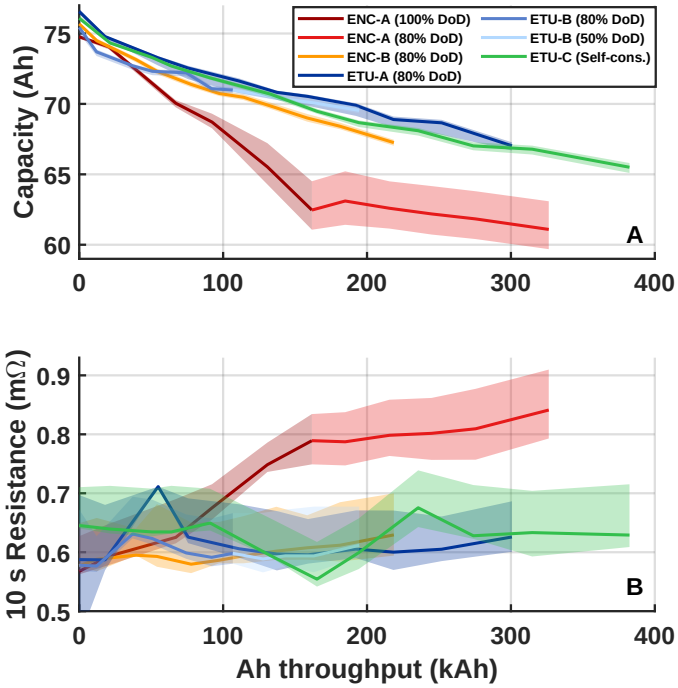

Figure 8. (A) Capacity dispersion in packs and (B) cell 10 s resistances at C/2 in module. The lines represent the medians and the paler zones the maximum and minimal limits.

Using the value of Δt, the voltage profile of each cell is extended along the time axis by the corresponding Δt, representing the time it would take for each cell to reach the cutoff voltage of 2.7 V. This mirrored projection allows for estimating the additional capacity each cell could have delivered. The extra capacity is then obtained by multiplying the average discharge current by Δt (Fig. 7).

For the batteries analyzed in this project, Fig. 8 illustrates the evolution of capacity and resistance dispersion across the different packs during the aging campaign. Among all the packs, only ENC-A exhibited significant capacity heterogeneity, with a spread of 3.4 Ah between the highest and lowest capacity cells toward the end of the test period. Notably, the capacity dispersion in ENC-A increased more sharply after reaching approximately 100 kAh of throughput. Even at similar median capacity levels, ENC-A showed greater variation compared to the other packs. Regarding the 10-second resistance measurements, only ENC-A demonstrated a marked increase in resistance, likely attributed to lithium consumption and SEI layer growth. Nevertheless, resistance dispersion remained relatively stable across all the tested battery packs.

3.2.2. *Impact of Capacity Dispersion on BMS Balancing Behavior*

To assess the impact of capacity dispersion on BMS operation, the number of balancing pulses during pause phases was counted over the course of the aging campaign for each battery. An example of these pulses is shown in the inset of Fig. 9A. As illustrated, the BMS of ENC-A exhibited a significantly higher number of balancing pulses compared to the other packs. Once the median SoH dropped to around 85% and the maximum SoH deviation between cells reached 3.8%, the balancing circuit began to activate more frequently, resulting in a sharp increase in pulse count up to the point of the profile change.

Following the profile change, the number of pulses increased slightly, driven by the higher voltage spread between cells at the new upper charge limit (around 4.0 V for 90% SoC compared to 4.2 V at 100% SoC). However, since the overall battery capacity remained relatively stable after this change, the increase in pulses progressed more gradually than it did under the original 100% DoD profile. In contrast, the BMS balancing activity in most of the other batteries remained low and largely unchanged throughout the campaign, intervening only to correct minor SoC imbalances.

For ETU-A, throughout the entire campaign, it experienced slightly more balancing during pauses compared to the other batteries (excluding ENC-A), as expected due to its higher capacity dispersion. However, around the 250 kAh mark, it underwent an abrupt increase in the number of balancing pulses. This occurred immediately after it reached its peak SoH dispersion of 1.38%. Nevertheless, this is not believed to be the root cause of the rise in pulse count, as the capacity dispersion did not increase afterward. The increase is instead attributed to a traditional SoC imbalance following a complete characterization profile during which both individual modules were disconnected.

Analyzing the distribution of balancing pulses per cell for ENC-A reveals an interesting pattern: the most degraded cells tend to be balanced less frequently, as illustrated in Fig. 10. Specifically, the 5th and 6th cells, which have the lowest capacities, are among the least frequently balanced, ranking first and third from the bottom, respectively (Fig. 10B). In contrast, the outermost cells, such as the 14th, which exhibit higher capacities, undergo significantly more balancing. For instance, the 14th cell experienced 14 times more balancing pulses than the 5th.

To better interpret the number of balancing pulses, it is useful to track the voltage of the limiting cell during cycling. Fig. 11A shows which cells limited the charge cycles throughout aging. The first position, shown in red, indicates the cell that reached the upper voltage threshold first, while the 14th position corresponds to the cell that remained furthest from the threshold at the end of each charge cycle (lowest voltage). It is evident that towards the end of the campaign, the most and least limiting cells remain stable. The 6th cell most frequently reached the voltage limit first, indicating it was the most limiting. This cell also had one of the lowest capacities and highest resistance val-

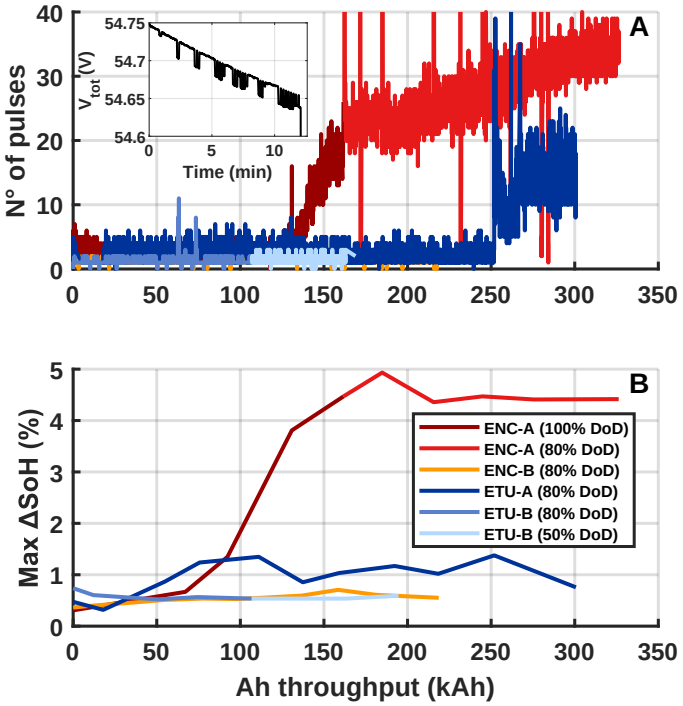

Figure 9. (A) Number of balancing pulses during the 30-minute pauses and (B) maximum ΔSoH.

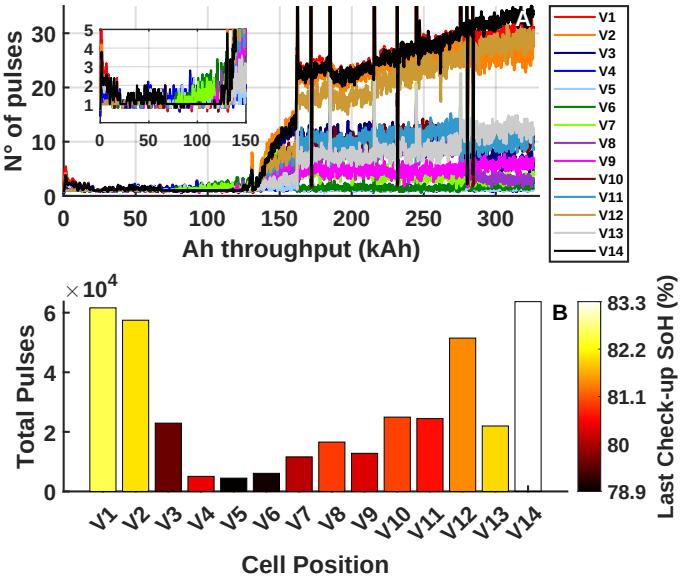

Figure 10. (A) Number of balancing pulses during the 30-minute pause for the cells in ENC-A and (B) cumulative number of balancing pulses per cell with respect to the SoH.

ues, as shown in Fig. 12. In contrast, the 13th cell, often the least limiting, showed one of the highest capacities and lowest resistance values by the end of the test.

Although the 6th cell was typically the first to reach the voltage threshold during charging, effectively acting as the limiting cell, its higher resistance led to a significant voltage drop during the relaxation phase. As a result, its post-relaxation voltage was often lower than that of other cells, meaning it required little balancing despite limiting the charge process.

Moreover, as seen in Fig. 11B, the end-of-charge voltage difference at the beginning of the campaign started off high, until around 100 kAh exchanged. During this period, when capacity dispersion was not elevated, the number of balancing pulses per pause was low and were triggered by the SoC imbalance. Between the 100 kAh mark and up to the profile change, indicated by the black dashed line, the capacity dispersion increased and the number of balancing pulses rose abruptly (135 kAh).

After the profile change, a sudden increase in the voltage difference ΔV_{lim} between the cells and the limiting one was observed. This is attributed to the inherently higher cell-to-cell voltage differences at 80% SoC compared to a fully charged pack. Since the battery did not experience significant degradation after this change, ΔV_{lim} remained stable. However, the number of balancing pulses stayed high. This suggests that the imbalance detected by the BMS was due to capacity dispersion, which cannot be resolved by the balancing strategy designed for SoC equalization.

An interesting observation is the impact of the higher resistance of the 14th cell at the beginning of the campaign. This cell initially limited the charge cycles, as all other cells had similar capacities but lower resistance values, as seen in Fig. 12. However, around the 130 kAh mark, capacity dispersion between the cells increased abruptly, which activated the balancing circuits and significantly changed the ranking of the limiting cells.

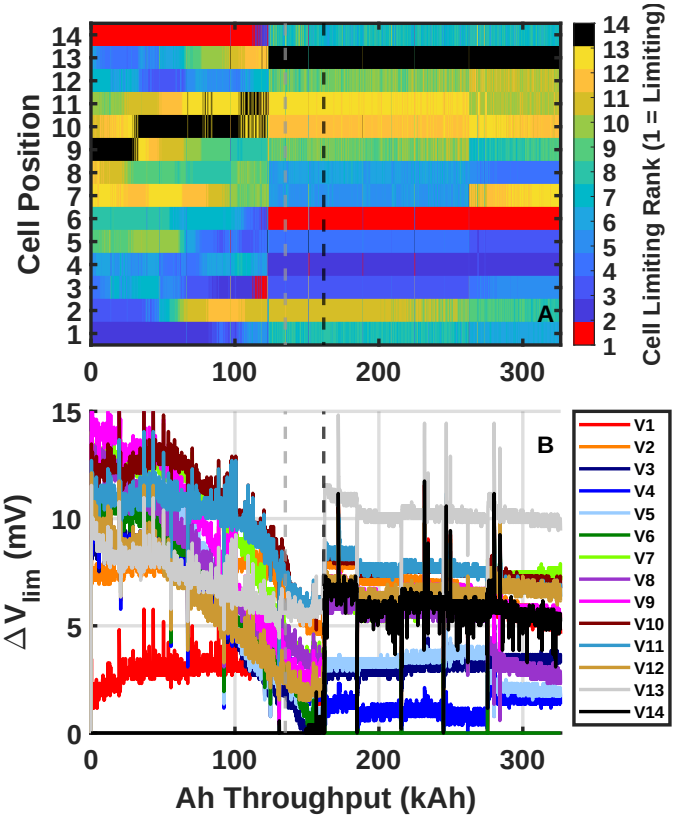

Figure 11. (A) End-of-charge voltage ranking for ENC-A. (B) Voltage difference ΔV_{lim} to the limiting cell. Dashed lines: profile change (black) and abrupt pulse increase (grey).

Fig. 12 exhibits both the 10-second resistances and the SoH per cell in ENC-A. As seen in the figure, the SoH distribution was homogeneous at the beginning of the campaign. However, towards the end, the cells located in the center showed a more pronounced capacity loss. Regarding the resistances, apart from the outermost cells, which exhibited slightly higher values due to the internal module harness adding to the perceived resistance, all cells were initially homogeneous, similar to the capacity distribution. However, over the course of the campaign, the central cells developed slightly higher resistances than the exterior ones, mirroring the capacity trend. This effect is believed to result from the greater difficulty center cells face in dissipating heat, causing them to operate at higher average temperatures,

surpassing 40°C.

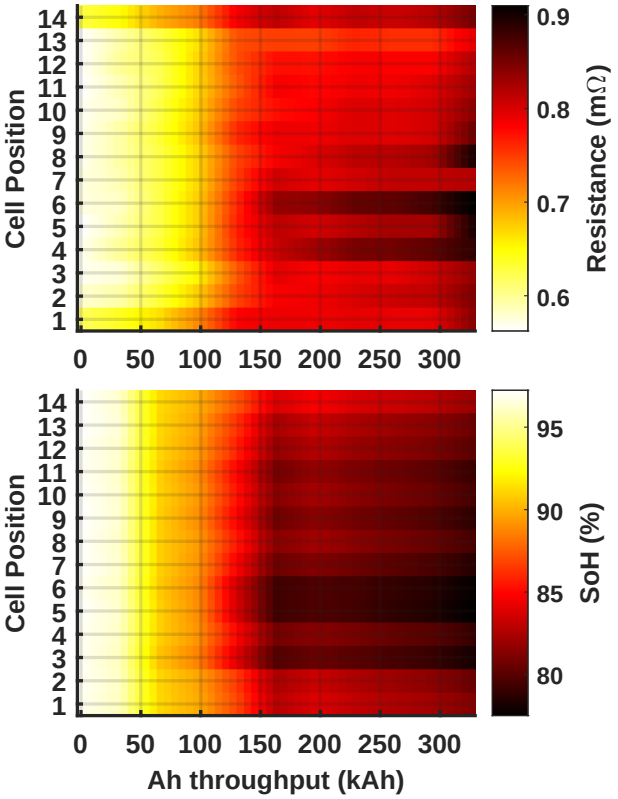

Figure 12. 10-second resistance and SoH heatmaps for ENC-A.

Fig. 13 shows the mean number of balancing pulses as a function of the estimated capacity difference between each cell and the cell with the lowest capacity, measured during the discharge phase for ENC-A. The mean was calculated using the 40 pauses following a characterization profile. As seen in the figure, a trend can be identified. Most cells, after having reached a 1 Ah difference from the limiting cell, undergo an increasing number of balancing pulses. It is noticeable, however, the abrupt change experienced for most cells, right after the profile change from 100% DoD to 80% DoD. The region where cells exhibit a high capacity difference relative to the limiting cell but a low mean number of balancing pulses corresponds to data recorded before the profile change, as highlighted in the zoomed-in plot. This shows that for a given end of charge voltage, there could be an expected trend for the number of balancing pulses. In the same figure, for the region showing a homogeneous battery pack capacity (low Q differences) the cells are balanced, but most likely to address a measured SoC variation, as originally intended by the BMS.

4. CONCLUSIONS

Due to the technical challenges and complexity involved in aging Li-ion batteries at the pack level, few studies provide aging data from systems that closely resemble real-world applications. In this work, a robust aging test bench was presented, and five second-life Li-ion battery packs were aged using a BMS with passive balancing capabilities. Our study is particularly interesting because we show aging data from battery packs while analyzing the interaction with the BMS and considering the heterogeneity within the packs.

One conclusion drawn from this in-depth analysis of pack dispersion and its influence on the BMS balancing function is that, while the BMS visibly attempts to compensate for cell imbalance, it ultimately fails to achieve its objective. This is because the imbalance does not stem from a simple SoC dispersion but

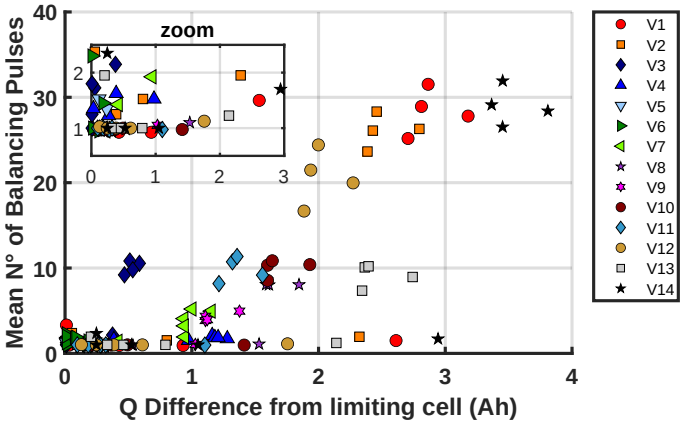

Figure 13. Mean number of balancing pulses with respect to the capacity difference between a given cell and the limiting one with the lowest capacity.

rather from an inherently uncorrectable issue, capacity dispersion, at least within the constraints of the given BMS architecture. A BMS capable of addressing capacity dispersion by selectively utilizing certain cells more than others could offer a smart solution to mitigate this issue, specially in case of second life batteries. However, such a BMS would be more costly due to the electronics capable of isolating certain cells.

Moreover, the observed correlation between the number of balancing pulses and capacity dispersion presents an intriguing idea for estimating capacity dispersion simply by tracking these pulses throughout the battery pack's lifespan and is a perspective of this work. In order to develop such a method, the number of balancing pulses should be measured at multiple end-of-charge voltages.

5. ACKNOWLEDGMENTS

This work was funded by the B2LIVE project, with support from the OCCITANIE Region and SNAM.

6. REFERENCES

[1] E. Michelini, P. Höschele, F. Ratz, M. Stadlbauer, W. Rom, C. Ellersdorfer, and J. Moser, "Potential and most promising second-life applications for automotive lithium-ion batteries considering technical, economic and legal aspects," Energies, vol. 16, no. 6, Art. no. 2830, 2023, doi: 10.3390/en16062830.

[2] I. San Martín, E. Braco, Á. Martin, P. Sanchis, and A. Ursúa, "Integration of second-life batteries in residential microgrids and fast charging stations," in Proc. IEEE Int. Conf. Environment and Electrical Engineering and IEEE Industrial and Commercial Power Systems Europe (EEEIC / I&CPS Europe), 2022, pp. 1–6, doi: 10.1109/EEEIC/ICPSEurope54979.2022.9854414.

[3] L. Albuquerque et al., "Projet B2LIVE (Batteries de 2nde vie au Lithium Ion à Vieillissement caractérisé par Expérimentation)", 2023, hal-04505925.

[4] M. Hassini, "Batteries de seconde vie dans une application de recharge de véhicules : Maîtrise des performances", Ph.D. thesis, 2024, doi: 10.13140/RG.2.2.30526.70724.

[5] L. Albuquerque et al., "Banc de caractérisation et de cyclage batteries," 2023, hal-04505960. Available: ut3-toulouseinp.hal.science/hal-04505960v1

[6] W. Gao et al., "Comprehensive study of the aging knee and second-life potential of the Nissan Leaf e+ batteries," Journal of Power Sources, vol. 613, p. 234884, 2024, doi: 10.1016/j.jpowsour.2024.234884.

[7] M. Naguib, P. Kollmeyer, and A. Emadi, "Lithium-ion battery pack robust state of charge estimation, cell inconsistency, and balancing: Review," IEEE Access, vol. 9, pp. 50570–50582, 2021, doi: 10.1109/ACCESS.2021.3068776.

[8] M. Hassini et al., "Capacity Dispersion and Impact of Outliers in a Second Life Battery," in 2023 IEEE Vehicle Power and Propulsion Conference (VPPC), 2023, pp. 1-4, doi: 10.1109/VPPC60535.2023.10403384.